Loss Mechanisms in Thick-Film Low-Bandgap Polymer Solar Cells

Cephas E. Small, Sai-Wing Tsang, Song Chen, Sujin Baek, Chad M. Amb, Jegadesan Subbiah, John R. Reynolds, and Franky So**

Polymer bulk heterojunction solar cells based on low bandgap polymer:fullerene blends are promising for next generation low-cost photovoltaics. While these solution-processed solar cells are compatible with large-scale roll-to-roll processing, active layers used for typical laboratory-scale devices are too thin to ensure high manufacturing yields. Furthermore, due to the limited light absorption and optical interference within the thin active layer, the external quantum efficiencies (EQEs) of bulk heterojunction polymer solar cells are severely limited. In order to produce polymer solar cells with high yields, efficient solar cells with a thick active layer must be demonstrated. In this work, the performance of thick-film solar cells employing the low-bandgap polymer poly(dithienogermole-thienopyrrolodione) (PDTG-TPD) was demonstrated. Power conversion efficiencies over 8.0% were obtained for devices with an active layer thickness of 200 nm, illustrating the potential of this polymer for large-scale manufacturing. Although an average EQE > 65% was obtained for devices with active layer thicknesses > 200 nm, the cell performance could not be maintained due to a reduction in fill factor. By comparing our results for PDTG-TPD solar cells with similar P3HT-based devices, we investigated the loss mechanisms associated with the limited device performance observed for thick-film low-bandgap polymer solar cells.

1. Introduction

Polymer bulk heterojunction (BHJ) solar cells, which have the potential to provide low cost energy harvesting, are receiving much attention in research and development.[1–4] We recently reported over 8% power conversion efficiency (PCE) in an inverted structure, which is crucial for demonstrating the viability of this technology for large-scale roll-to-roll (R2R) processing.[5,6] Despite this performance for laboratory-scale inverted devices, the cell geometry is not the only factor determining their compatibility for large-scale manufacturing. Other key factors such as the use of indium tin oxide (ITO) and vacuum-processed metal electrodes are elements of the laboratory-scale process that are not attractive for future organic photovoltaic (OPV) technology due to their high cost, higher embodied energy, and increased energy payback time for PV modules.[7,8] Current research efforts have focused on demonstrating ITO-free R2R-processed polymer solar cells that completely avoid vacuum-processing steps.[9–11] Another key factor for improving the large-scale R2R processing compatibility of polymer solar cells is the active layer thickness required to ensure high manufacturing yields in PV modules.[12] Most high efficiency laboratory-scale devices demonstrated have an active layer with a thickness of about 100 nm which is too thin for R2R processing to ensure a pinhole-free film. Obtaining high efficiency devices with active layers thicker than 200 nm is critical for commercialization.[12,13]

In addition to the thickness requirement associated with large-scale R2R processing, increased active layer thickness is also required for optimal light harvesting to produce high efficiency polymer solar cells. Presently, solar cells with enhanced light absorption have been demonstrated by employing low bandgap polymers with optical bandgaps between 1.2 and 1.7 eV.[14–18] To obtain a high FF in these high efficiency cells, with the exception of poly(3-hexylthiophene) (P3HT) BHJ solar cells, the active layer thickness used is typically less than 100 nm. However, due to optical interference effects, a high EQE can only be obtained in these devices when the thickness exceeds 200 nm.[19] Therefore, despite their high PCEs, low bandgap polymer solar cells do not take advantage of the true light harvesting potential of the polymer used in such thin-film devices. The average EQE is expected to increase for solar cells with a thicker active layer due to enhanced light absorption and optimum light management. Therefore, to meet the large-scale

Dr. C. E. Small, Dr. S.-W. Tsang, Dr. S. Chen, S. Baek, Dr. J. Subbiah, Prof. F. So
Department of Materials Science and Engineering
University of Florida
Gainesville, FL 32611, USA
E-mail: fso@mse.ufl.edu
Dr. C. M. Amb
The George and Josephine Butler Polymer Research Laboratory
Department of Chemistry
Center for Macromolecular Science and Engineering
University of Florida
Box 117200, Gainesville, FL 32611, USA
Prof. J. R. Reynolds
School of Chemistry and Biochemistry
School of Materials Science and Engineering
Georgia Institute of Technology
Atlanta, GA 30332-0400, USA
E-mail: reynolds@chemistry.gatech.edu

DOI: 10.1002/aenm.201201114

R2R processing requirement and ultimately realize optimum light absorption, polymer solar cells with a thicker active layer must be demonstrated.

In the past, demonstrating high efficiency polymer solar cells with a thick active layer has been a challenge. Previous work has focused on obtaining high hole mobilities in low bandgap polymers when blended with fullerene. This has been achieved by developing novel polymer structural designs and by improving the nanoscale morphology of polymer:fullerene BHJ films.[20,21] The improved carrier transport helps alleviate the buildup of photogenerated carriers in devices with thicker active layer, which decreases the probability of carrier recombination and, consequently, enhances the carrier collection efficiency.[20–25] While this approach has been successful for polymer solar cells such as poly(3-hexylthiophene):[6,6]-phenyl-C61 butyric acid methyl ester (P3HT:$PC_{61}BM$), solar cells employing low bandgap conjugated polymers with fused donor–acceptor moieties show significant reductions in FF and PCE with increasing BHJ film thickness despite showing high efficiencies for thin-film dev ices.[20,23,26–30] Understanding the underlying mechanism of the FF reduction and, consequently, achieving high efficiency in low bandgap polymer solar cells with a thicker active layer is particularly important for the development of low-cost, high efficiency polymer solar cells for commercial applications.

In this work, we investigated the photovoltaic characteristics of polymer solar cells by employing the low-bandgap polymer poly(dithieno[3,2-b:2,3-d]germole thieno[3,4-c]pyrrole-4,6-dione) (PDTG-TPD).[18] In our previous work, we demonstrated the PCEs of these cells can be as high as 8.1% with an active layer thickness of about 100 nm.[5,6] Here, we demonstrate that increasing the active layer thickness (L) up to 200 nm yielded devices with a PCE above 8.0%, which shows the viability of the PDTG-TPD:[6,6]-phenyl-C71 butyric acid methyl ester ($PC_{71}BM$) system for large-scale R2R processing. For devices with an active layer thickness > 200 nm we observed a marked reduction in FF and PCE, despite an average EQE above 65%. On the contrary, similar P3HT:$PC_{61}BM$ polymer solar cells showed almost no reduction in FF for devices with an active layer thickness up to 453 nm. Interestingly, similar space-charge limited (SCL) hole mobility values (μ_h) were obtained for both polymer:fullerene BHJ films despite the difference in fill factor behavior with increasing active layer thickness. We interpret these results as follows: the broader absorption band for the PDTG-TPD:$PC_{71}BM$ system leads to increased charge carrier generation and increased space-charge buildup in the photoactive layer compared to P3HT:$PC_{61}BM$. The onset of space charge accumulation coincides with increased carrier recombination loss in the photoactive layer, which results in a significant FF reduction in devices with a thicker active layer.[22] Our analysis of the incident light intensity dependence of the FF, as well as our analysis of space-charge-limited (SCL) photocurrent in PDTG-TPD:$PC_{71}BM$ solar cells further supports our hypothesis.[31] In addition to space-charge effects, the reduced FF observed in thick PDTG-TPD:$PC_{71}BM$ solar cells is also attributed to a low carrier lifetime as compared to similar P3HT:$PC_{61}BM$ devices. Overall, our results indicate that recombination losses due to space-charge effects and low carrier lifetimes limit the performance of thick-film low-bandgap polymer solar cells.

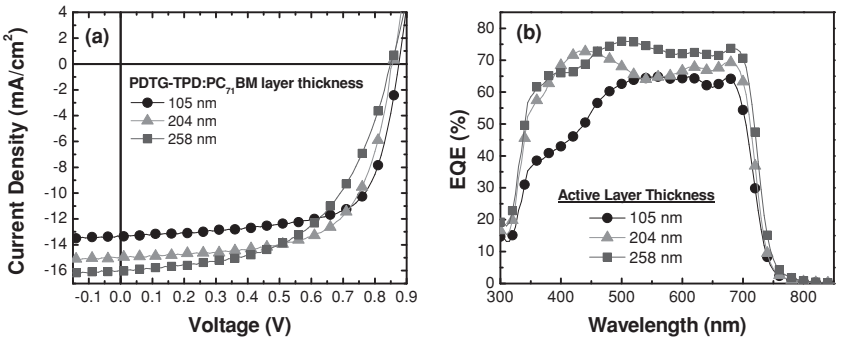

Figure 1. (a) Current density versus voltage characteristics for PDTG-TPD:$PC_{71}BM$ solar cells with 105 nm, 204 nm, and 258 nm-thick active layer. (b) Corresponding external quantum efficiency (EQE) spectra for the devices.

2. Results and Discussion

2.1. PDTG-TPD Solar Cell Performance

Figure 1 shows the photocurrent density–voltage (J–V) characteristics and the corresponding external quantum efficiency (EQE) spectra for inverted PDTG-TPD:$PC_{71}BM$ solar cells with 105 nm, 204 nm, and 258 nm-thick active layers. Figure 1a shows that the short-circuit current density (J_{sc}) increases with increasing active layer thickness due to enhanced light absorption, with the highest J_{sc} of 16.1 mA cm^{-2} obtained for the device with an active layer thickness of 258 nm. The integrated current density from the EQE spectra, shown in Figure 1b, is consistent with the measured J_{sc} with 5% deviation. The difference in the EQE spectra is due to optical interference effects between the incident light and light reflected from the Ag back electrode.[19] For devices with thickness $L \geq 200$ nm, the interference effects no longer affect the photocurrent density of the device and the active layer absorbs almost all of the incident light below 700 nm, resulting in EQEs above 70% from 400 nm to 700 nm.

Table 1 summarizes the average solar cell parameters for the PDTG-TPD:$PC_{71}BM$ devices with an active layer thickness varying from 90 nm to 409 nm. The reduction in FF observed for PDTG-TPD solar cells with increasing active layer thickness is the major factor limiting the device performance. A power conversion efficiency (PCE) of 7.9% is obtained for the device with a 105 nm thick active layer, which is consistent with our previously report.[5,6] The efficiency remains constant for devices with $L \leq 204$ nm, with an average PCE of 8.2% being obtained for devices with an active layer thickness of 204 nm. Above 200 nm, the FF reduction becomes significant, dropping from 69% in 105 nm film to 42% in 409 nm film. The performance for PDTG-TPD:$PC_{71}BM$ solar cells was then compared to similar devices based on P3HT:$PC_{61}BM$, which is a well studied material

DOI: 10.1002/aenm.201201114

Table 1. Averaged solar cell performance for PDTG-TPD:$PC_{71}BM$ devices with various active layer thickness under initial AM 1.5G solar illumination.

Active Layer Thickness	J_{sc} (mA cm^{-2})	J_{sc} (EQE) (mA cm^{-2})	V_{oc} (V)	FF (%)	PCE (%)
90 nm	12.5 +/–0.1	12.3	0.88	68.5 +/–0.1	7.5 +/–0.1
105 nm	13.3 +/–0.2	13.0	0.87	68.7 +/–0.3	7.9 +/–0.1
153 nm	13.5 +/–0.4	13.5	0.86	68.1 +/– 0.3	8.0 +/–0.2
204 nm	14.9 +/–0.3	14.7	0.86	64.5 +/–0.7	8.2 +/–0.2
258 nm	16.1 +/–0.2	16.0	0.85	54.1 +/–0.9	7.4 +/–0.1
409 nm	15.2 +/–0.1	14.9	0.82	41.6 +/–0.9	5.2 +/–0.1

system for investigating the active layer thickness dependence of the efficiency in laboratory-scale and large-scale R2R processed polymer solar cells.[20,21,32] The detailed solar cell performance for P3HT:$PC_{61}BM$ devices with active layer thickness from 100 nm to 453 nm can be found in Supporting Information (see Figure S1). **Figures 2**a and b show the average FF and average EQE as a function of active layer thickness for both PDTG-TPD and P3HT solar cells. For PDTG-TPD solar cells, a high average FF can only be obtained for devices with $L \leq 204$ nm. In contrast, a FF ≥ 65% was observed for P3HT:PC_{61} BM solar cells with $L \leq 453$ nm. In terms of the average EQE, only thick-film PDTG-TPD:PC_{71} BM solar cells with $L \geq 204$ nm was capable of reaching an average EQE of 65%.

In previous work, the reduction in FF for thick-film devices was attributed to polymer solar cells with low carrier mobility such as MDMO-PPV:$PC_{61}BM$.[22] The low mobility increases the chances of carrier recombination and therefore reduces the FF. We measured the space-charge-limited (SCL) hole mobility from PDTG-TPD:$PC_{71}BM$ single-carrier devices and compared those values with the mobility values for P3HT:$PC_{61}BM$ solar cells (see Supporting Information, Figure S2). The hole mobility values for the 105 nm and 409 nm-thick PDTG-TPD:$PC_{71}BM$ devices were 3.4×10^{-3} cm^2 V^{-1} s^{-1} and 2.3×10^{-3} cm^2 V^{-1} s^{-1}, respectively. These values are comparable with hole mobility values found for optimized P3HT:$PC_{61}BM$ solar cells reported in the literature.[20,21] It suggests that the reduction in device performance in thick film PDTG-TPD:$PC_{71}BM$ solar cells is not due to any reduction in carrier mobility.

To determine the root cause for the reduction in FF observed in thick-film PDTG-TPD:$PC_{71}BM$ solar cells, the EQE spectra for the thin-film and thick-film devices were measured under different values of internal electric field.[33] **Figure 3** shows the field-dependent EQE spectra for devices with 105 nm, 204 nm, 258 nm, and 409 nm-thick active layers, respectively. By measuring the EQE as a function of internal electric field (E), approximated as $E = {}^{(V_{oc}-V)}/_{L}$, the effect of series resistance can be eliminated. For the device with an active layer thickness ≤ 204 nm, increasing the applied field from 20 kV cm^{-1} to 70 kV cm^{-1} leads to a uniform enhancement in EQE across the entire spectral range. The increased applied field enhances the extraction of photogenerated charges equally across the EQE spectrum. Interestingly, for devices with $L > 204$ nm, a stronger field-dependent enhancement in EQE is observed in the spectral range from 500 to 750 nm when the applied field is increased from 20 kV cm^{-1} to 70 kV cm^{-1}. This wavelength range corresponds to the absorption spectrum for a pristine PDTG-TPD film.[18] For devices with a thick active layer, the build-up of charges in PDTG-TPD:$PC_{71}BM$ will hinder charge collection and contribute to the FF reduction in thick solar cells.

The limited charge collection observed for thick-film PDTG-TPD solar cells measured at low field results in reduced photocurrent in this field regime. **Figure 4** shows the normalized photocurrent density-electric field (J_L-E) curves for PDTG-TPD:$PC_{71}BM$ solar cells with increasing active layer thickness. For inverted PDTG-TPD:$PC_{71}BM$ solar cells with thickness ≤ 204 nm, the shapes of the J_L-E curves are identical. In this thickness regime, the internal electric field effectively extracts photogenerated charges from the active layer. For inverted devices with $L >$ 204 nm, a change in the J_L-E profile is observed. In this thickness regime, a reduction in photocurrent is observed in the low field regime. The internal electric field is no longer able to efficiently extract photogenerated charges out of the active layer. By comparison, the J_L-E profiles for P3HT:$PC_{61}BM$ solar cells are identical for devices with thickness up to 453 nm (see Supporting Information, Figure S3). Based on this result, the reduced FF observed in PDTG-TPD:$PC_{71}BM$ solar cells with thicker active layer can be attributed to two factors: (1) the reduction in internal electric field due to increased active layer thickness L, and (2) the reduced photocurrent at low electric field due to limited charge collection. The results presented in Figures 3 and 4 provide evidence that space-charge accumulation contributes to the limited charge collection and reduced FF observed in thick-film PDTG-TPD:$PC_{71}BM$ solar cells. We also expect increased recombination loss in thick-film devices since carriers have to traverse a longer distance to be collected. To better understand the loss mechanisms in thick-film low-bandgap polymer solar cells, a detailed study on space-charge limited (SCL) and recombination limited photocurrent is presented herein.

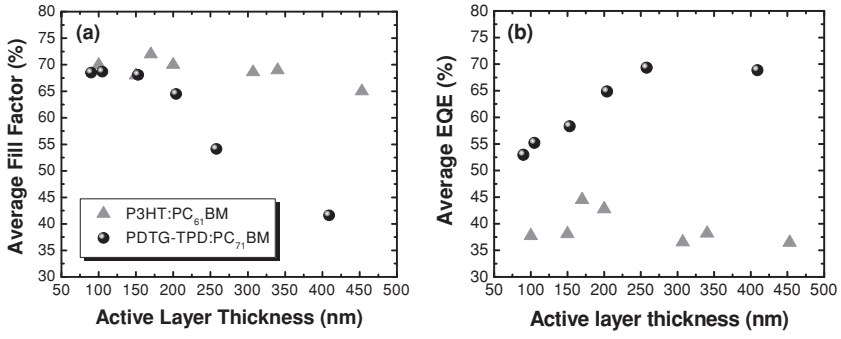

Figure 2. (a) Average fill factor and (b) average EQE versus active layer thickness for PDTG-TPD:$PC_{71}BM$ and P3HT:$PC_{61}BM$ solar cells. The average EQE was calculated over the wavelength range of the EQE spectra for PDTG-TPD and P3HT solar cells.

2.2. Loss Mechanisms in Thick-Film PDTG-TPD:$PC_{71}BM$ Solar Cells

In comparing P3HT and PDTG-TPD, a significant difference between these two

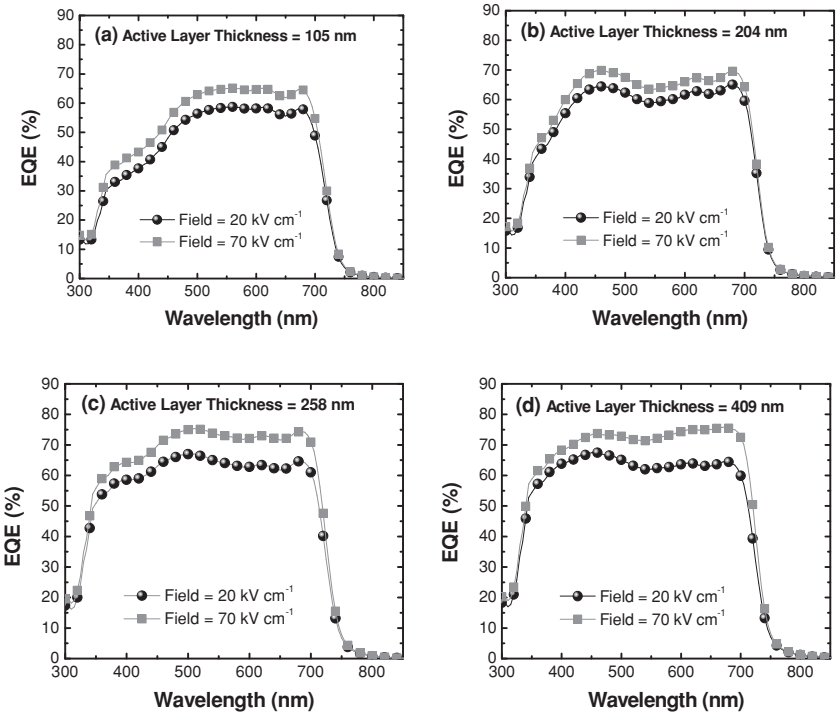

Figure 3. Field-dependent EQE spectra for PDTG-TPD:PC_{71}BM solar cells with (a) 105 nm, (b) 204 nm, (c) 258 nm and (d) 409 nm-thick active layer. The EQE spectra were measured at internal electric field values of 20 kV cm^{-1} and 70 kV cm^{-1}.

polymers is the broader absorption spectra absorption in PDTG-TPD due to its lower optical bandgap ($E_{gap} \approx 1.7$ eV).[18] The UV-visible-NIR absorption spectra for P3HT:PC_{61}BM and PDTG-TPD:PC_{71} BM solar cells along with the photon flux for an AM 1.5G solar spectrum are shown in **Figure 5**a. From the solar spectrum, an integrated photon flux of 1.6×10^{17} cm^{-2} s^{-1} is obtained for a wavelength range of 400 nm–800 nm. A larger fraction of this photon flux is absorbed by PDTG-TPD compared to the P3HT due to its broader absorption spectrum. Figure 5b shows the calculated percentage of the AM 1.5G solar spectrum absorbed for PDTG-TPD and P3HT solar cells as a function of the active layer thickness, which was varied from ~50 nm to 250 nm in the calculation. Here, these spectra were obtained from results of optical modeling using the n and k optical constants for each layer in the actual devices.[34] Based on the results, PDTG-TPD:PC_{71} BM solar cells have over 30% more absorption than that in P3HT:PC_{61} BM solar cells.

Due to its higher light absorption and higher rate of forming photogenerated charge carriers, it is obvious that thick-film low-bandgap polymer solar cells require more efficient charge collection to prevent space-charge from accumulating in the active layer. The onset of space-charge accumulation in polymer BHJ solar cells occurs when the rate of hole generation in the polymer is greater than the rate at which those carriers can be extracted out of the active layer.[25,31] The resulting space-charge effect screens the electric field in the active layer, resulting in reduction of the field in the BHJ film.[22] This reduction in electric field would negatively impact the charge carrier transport and extraction in polymer solar cells. The issue of SCL photocurrent in polymer solar cells with thick active layers has been addressed with a model first proposed by Goodman and Rose.[31] The space-charge limit is reached when the effective photocurrent (J_{ph}) generated is equal to or greater than the value shown in the following equation:[31,35]

$$j_{ph}^{SCL} = q\left(\frac{9\varepsilon_0\varepsilon_r\mu_h}{8q}\right)^{1/4} G^{3/4} V^{1/2} \quad (1)$$

where q is the electron charge, $\varepsilon_0\varepsilon_r$ is the dielectric permittivity, μ_h is the hole mobility, and G is the generation rate of free carriers. The value of J_{ph} is determined experimentally as $J_{ph} = J_L - J_D$, where J_L and J_D are the measured photocurrent density and dark current density, respectively.

To study the role space-charge accumulation plays in PDTG-TPD:PC_{71}BM solar cells with a thick active layer, we employed the SCL photocurrent model to confirm that the electrostatic space-charge limit was reached in our thick devices. We compared the results for PDTG-TPD:PC_{71}BM solar cells with similar devices based on P3HT:PC_{61}BM, since P3HT solar cells provide a model system for studying space-charge effects.[20,21] The effective photocurrent J_{ph}, normalized to the saturation photocurrent $J_{sat} = qG_{max}L$, was plotted on a double logarithmic scale against the effective voltage across the device, given by $V_{eff} = V_0 - V$. Here, V_0 is defined as the voltage where $J_{ph} = 0$ and is slightly larger than V_{oc}.[25] This "corrected" photocurrent analysis is a widely used tool for analyzing recombination loss processes in organic solar cells.[36–38] **Figure 6**a shows the results for the PDTG-TPD:PC_{71}BM solar cells with 105 nm, 258 nm and 409 nm-thick active layer. For the device with a 105 nm-thick active layer, two different voltage regimes can be observed. For $V_{eff} < 0.30$ V, J_{ph} steadily increases with voltage due to the

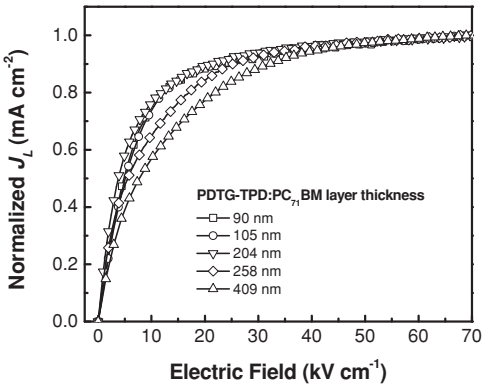

Figure 4. Normalized photocurrent density (J_L) as a function of internal electric field $E = {}^{(V_{oc}-V)}/_{L}$ for inverted PDTG-TPD:PC_{71}BM devices with increasing active layer thickness.

DOI: 10.1002/aenm.201201114

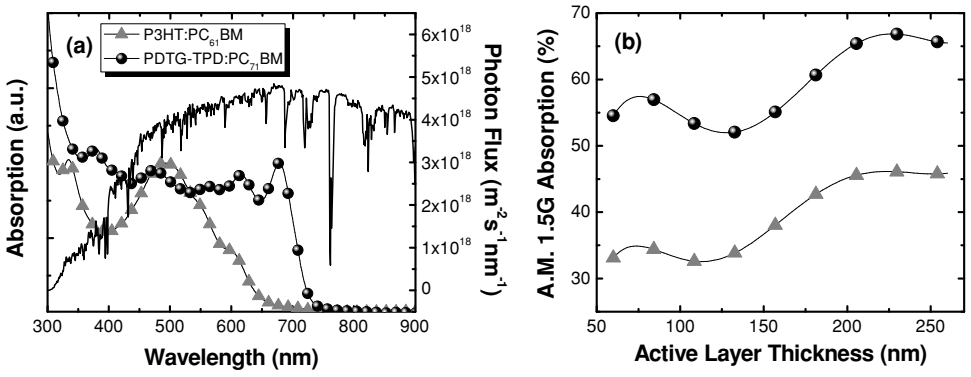

Figure 5. (a) UV-Vis-NIR absorption spectra for PDTG-TPD:$PC_{71}BM$ and P3HT:$PC_{61}BM$ solar cells. The photon flux for the AM 1.5G solar spectrum is shown for the same wavelength range. (b) The corresponding calculated AM 1.5G absorption versus active layer thickness for the devices. The *n* and *k* optical constants for PDTG-TPD:$PC_{71}BM$ and P3HT:$PC_{61}BM$ were obtained by ellipsometry measurements.

competition between diffusion and drift for photo-generated carrier transport at low field. For $V_{eff} > 0.30$ V, the photocurrent saturates with increasing voltage. In this saturation regime, the internal field is strong enough to efficiently extract photogenerated carriers and the high field is responsible for the dissociation of *e-h* pairs. The voltage corresponding to the short circuit condition falls within the saturation regime, indicating that the high J_{sc} and FF obtained for this device is due to efficient charge collection by the internal electric field. For the device with a 105 nm active layer, space charge effects were not observed based on the data shown in Figure 4a. As the active layer thickness for PDTG-TPD cells increased above 200 nm, a square-root effective voltage dependence on J_{ph} is observed. This $J_{ph} \propto V^{1/2}$ corresponds to the onset of space-charge limited photocurrent in thick PDTG-TPD cells assuming a $J_{ph} \propto G^{3/4}$ dependence is also observed.[38] The solid lines in Figure 6a correspond to $J_{ph} \propto V^{1/2}$. For the 409 nm-thick device, the $J_{ph} \propto V^{1/2}$ regime extends to the short circuit condition, which correlates well with the reduction in J_{sc} and FF observed in this device.

The normalized J_{ph}-V_{eff} curves for P3HT:$PC_{61}BM$ solar cells with 100 nm, 200 nm, and 453 nm-thick active layers are shown in Figure 6b. In contrast with the results obtained for the thick PDTG-TPD:$PC_{71}BM$ devices, the curves for all three P3HT:$PC_{61}BM$ solar cells look very similar despite the increase in the active layer thickness. These results correlate well with the high FFs of 65% to 68% obtained for the P3HT:$PC_{61}BM$ devices. Since the onset of the $J_{ph} \propto V^{1/2}$ regime was not observed in the P3HT:$PC_{61}BM$ solar cells, the photocurrent in these devices was not space-charge limited despite the increase in active layer thickness.

To confirm that space-charge accumulation was contributing to the reduction in efficiency in PDTG-TPD:$PC_{71}BM$ solar cells with a thick active layer, we measured the solar cell performance as a function of incident light intensity for a thin-film and thick-film device. Early studies of space charge effects in organic solar cells based on poly(*p*-phenylene vinylene) (PPV) derivative:PCBM blends demonstrated the onset of SCL photocurrent through light intensity-dependent measurements.[31] In the present work, we argue that the reduction in FF observed in PDTG-TPD is due to SCL photocurrent in the thick-film device. Although the square-root dependence of the effective voltage on J_{ph} is an indication of space-charge-limited photocurrent, it may also correspond to recombination-limited photocurrent. In this case of recombination-limited photocurrent, the recombination of charge carriers becomes significant as the mean free electron or hole drift length becomes less than the active layer thickness.[38,39] Since recombination-limited photocurrent is given as:

$$J_{ph} \propto G\sqrt{\mu\tau}\sqrt{V} \tag{2}$$

where τ is the lifetime of free carriers, it is possible to determine whether space-charge-limited or recombination-limited photocurrent is limiting the FF of the solar cell by analyzing the light intensity dependence of the photocurrent.[38,39] While the SCL photocurrent scales with a 3/4 power dependence on light intensity (Equation 1), the photocurrent scales linearly in the absence of space-charge effects (Equation 2).

The dependence of J_{ph} and FF on incident light intensity (P_0) was plotted for the 105 nm and 409 nm-thick PDTG-TPD:$PC_{71}BM$ solar cells (see **Figure 7**). Neutral density filters were used to control the incident light intensity, which was varied from 11.4 to 100 mW cm^{-2}. The J_{ph}–P_0 data for the thin and thick PDTG-TPD:$PC_{71}BM$ devices, shown in Figure 7c, was extracted from the J_{ph}–V_{eff} curves shown in Figures 7a and b. For the solar cell with a 105 nm-thick active layer, J_{ph} showed a linear dependence on light intensity with the slope of the linear fit to

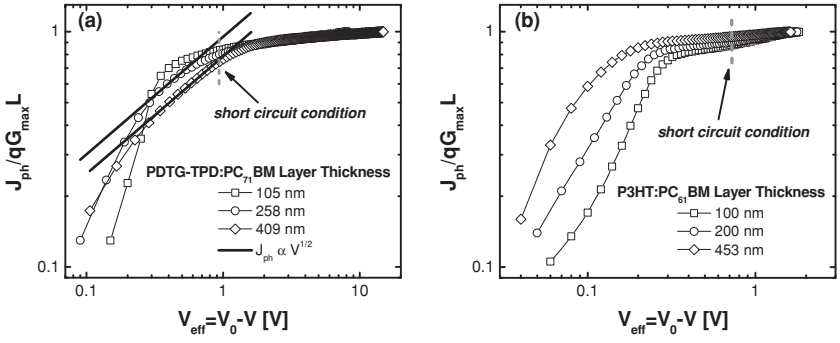

Figure 6. Effective photocurrent density (J_{ph}) normalized by $J_{sat} = qG_{max}L$ as a function of effective voltage (V_{eff}) under 100 mW cm^{-2} illumination for (a) PDTG-TPD:$PC_{71}BM$ cells with 105 nm, 258 nm, and 409 nm-thick active layer, and (b) P3HT:$PC_{61}BM$ cells with 100 nm, 200 nm, and 453 nm-thick active layer. Dashed lines highlight the value of V_{eff} corresponding the short-circuit condition ($V_{eff} = V_0$). The solid lines correspond to $J_{ph} \propto V^{1/2}$ fits of the photocurrent in the SCL regime for PDTG-TPD solar cells.

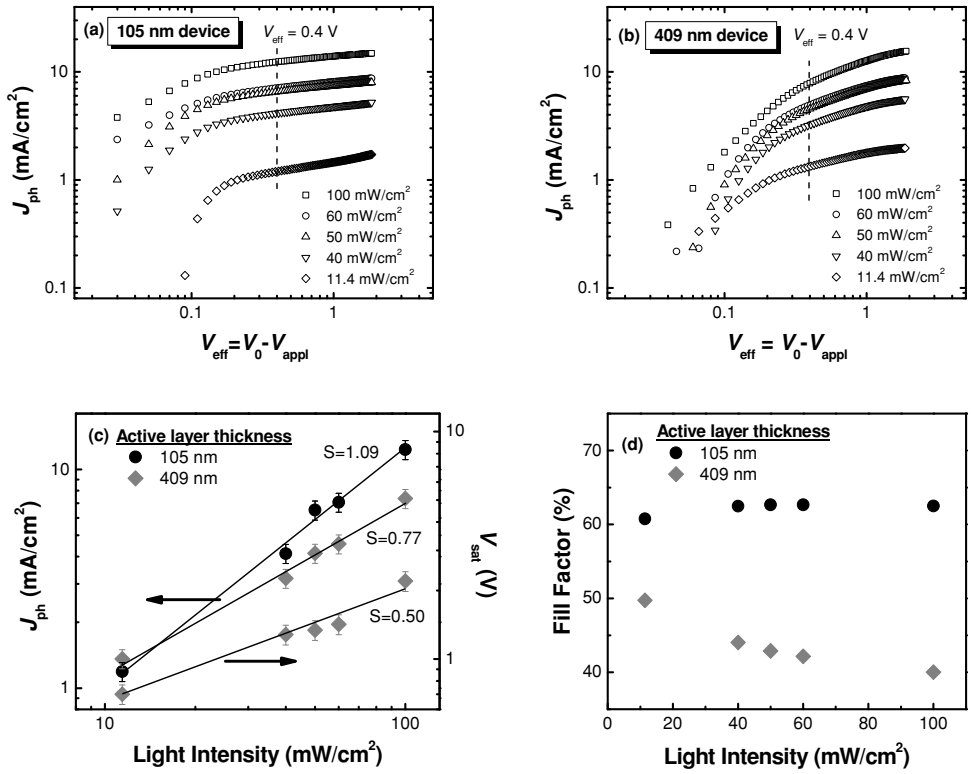

Figure 7. Light intensity dependent study for PDTG-TPD:$PC_{71}BM$ solar cells with thin and thick active layer. J_{ph}–V_{eff} curves for the (a) 105 nm-thick and (b) 409 nm-thick devices under various light intensities (from 11.4 to 100 mW cm^{-2}). (c) Effective photocurrent density (J_{ph}), saturation voltage (V_{sat}), and (d) fill factor as a function of incident light intensity for the same devices. The J_{ph}–P_0 curves shown in Figure 7c were measured at V_{eff} = 0.4 V.

the data equal to 1.09. In contrast, a slope of 0.77 is observed for the 409 nm-thick PDTG-TPD solar cell. The ~3/4 power dependence of J_{ph} on the incident light intensity confirms the occurrence of SCL photocurrent in PDTG-TPD:$PC_{71}BM$ solar cells at low bias. The dependence of the saturation voltage (V_{sat}) on incident light intensity provides further evidence, in which a slope of 0.50 is extracted from the V_{sat}–P_0 data.[31,38] To form a more clear physical picture, the light-intensity dependence of the FF was also analyzed and plotted in Figure 7d. The FF remained relatively constant with incident light intensity for the 105 nm-thick solar cell, which is expected since the device is not space-charge limited at P_0 = 100 mW cm^{-2} and the thickness is sufficiently thin to ensure efficient charge extraction. For the 409 nm-thick PDTG-TPD solar cell, a 24% enhancement in FF was observed as the incident light intensity was decreased from 100 mW cm^{-2} to 11.4 mW cm^{-2}. By lowering P_0 and, consequently, reducing the generation rate of charge carriers in the thick PDTG-TPD:$PC_{71}BM$ active layer, space-charge buildup was reduced. As a result, enhanced charge carrier collection and FF was observed in the solar cell. Despite this enhancement, the FF of the 409 nm-thick device at low light intensity does not reach the value obtained in the 105 nm device. This result indicates that the reduced photocurrent observed for thick-film devices, first shown in Figure 3, could not be completely recovered despite lowering the incident light intensity. There is still some degree of limited charge collection occurring in thick-film PDTG-TPD:$PC_{71}BM$ solar cells.

We note that the SCL photocurrent model employed in this work has two important assumptions. First, the SCL photocurrent model assumes that $\mu_h \ll \mu_e$ since the accumulation of slow carriers in the active layer is responsible for the space-charge limited being reached. For polymer solar cells, SCL photocurrent was first observed in systems with highly imbalanced mobilities.[22] In this work, we observed this effect for solar cells using a polymer showing high hole mobility and therefore having a much smaller carrier mobility imbalance. Nevertheless, our experimental results clearly indicate that space-charge accumulation contributed to the reduced FF and PCE observed in thick-film PTG-TPD:$PC_{71}BM$ solar cells. Furthermore, by calculating the active layer thickness at which $J_{ph} = J^{SCL}_{ph}$, the model predicts that the space-charge limit is reached when $L \approx 225$ nm.[31,35,40] This prediction correlates well with the reduced photocurrent observed for devices with $L > 200$ nm. The model also predicts that $G \propto \mu_h$ when $J_{ph} = J^{SCL}_{ph}$. Since PDTG-TPD:$PC_{71}BM$ solar cells have over 30% more photon absorption compared to P3HT devices, the carrier mobility required to alleviate space-charge effects in the low-bandgap polymer would be larger. Second, the model assumes that the loss observed in thick-film polymer solar cells is due to either SCL or recombination-limited photocurrent. However, these two loss processes are interrelated.[22] To determine if short-lived carriers in PDTG-TPD contributed to the reduced photocurrent observed in thick-film devices, we measured the carrier lifetimes for PDTG-TPD and P3HT solar cells.

DOI: 10.1002/aenm.201201114

Transient photovoltage (TPV) was used to characterize the carrier lifetime for the devices, as reported previously.[17] The carrier lifetimes for PDTG-TPD:$PC_{71}BM$ and P3HT:$PC_{61}BM$ solar cells were 1 μs and 8 μs, respectively. The slightly lower carrier lifetime for PDTG-TPD:$PC_{71}BM$ solar cells compared to similar P3HT:$PC_{61}BM$ devices results in more bimolecular recombination loss in thick film PDTG-TPD devices. Based on these results, we conclude that both SCL and recombination-limited photocurrent contributes to the losses observed in PDTG-TPD solar cells with thick active layer.

3. Conclusions

To conclude, the loss mechanism in thick-film PDTG-TPD:$PC_{71}BM$ solar cells have been investigated. For polymer solar cells with an active layer thickness up to 200 nm, efficiencies in excess of 8.0% were obtained for devices under AM 1.5G illumination at 100 mW cm^{-2}. For $L > 200$ nm, the SCL photocurrent regime is reached, leading to limited charge collection efficiency in the devices due to space-charge accumulation. The onset of space-charge accumulation also coincides with reductions in FF and hence power conversion efficiency in thick devices. These results indicate that although high efficiencies can be obtained in solar cells with low-bandgap conjugated donor-acceptor polymers, the high density of photogenerated charge carriers could severely limit the performance of solar cells with a thick active layer.

4. Experimental Section

The detailed synthesis, purification, and polymer characterization for PDTG-TPD has been reported elsewhere.[13] P3HT was purchased from Rieke Metals, Inc.. Both $PC_{61}BM$ and $PC_{71}BM$ used for solar cell fabrication were purchased from Solenne. For the inverted PDTG-TPD-based devices, the polymer and $PC_{71}BM$ were dissolved in chlorobenzene with 1:1.5 weight ratio and 5% volume ratio of 1,8-diiodooctane (DIO) was added as a processing additive to both solutions. The ZnO-PVP nanocomposite electron transporting layer, whose processing has been previous reported, was processed on indium tin oxide (ITO)-coated glass substrates.[5] The ITO substrates were first cleaned with detergent, ultrasonicated in DI water, acetone, and isopropyl alcohol, and subsequently dried under a nitrogen flow. The polymer-fullerene solutions were then spin-coated at various spin speeds to control active layer thickness and the resulting films were annealed at 80 °C for 30 minutes. Finally, thin films of MoO_3 (4 nm) and Ag (100 nm) were deposited through shadow masks via thermal evaporation. The active area of the device was 4.6 mm^2. For the P3HT:$PC_{61}BM$ solar cells, P3HT and $PC_{61}BM$ were dissolved in chlorobenzene with 1:1 (8 mg mL^{-1}:12 mg mL^{-1}) weight ratio. Thermally evaporated films of MoO_3 (Sigma Aldrich, 4 nm) and bathocuproine (BCP, 5 nm) were used for the anode and cathode interlayers, respectively. The P3HT:$PC_{61}BM$ solar cells had the following structure: ITO/MoO_3/P3HT:$PC_{61}BM$/BCP/Al. The active layer thickness was controlled by varying the spin-coating speed. The hole-only devices fabricated to extract hole mobility had the following structure: ITO/PEDOT:PSS/active layer/MoO_3/Ag. Current density-voltage measurements were carried out in air after encapsulation using a Keithly 4200 semiconductor system. For field-dependent EQE measurements, a bias was applied to the device using a current amplifier. For all EQE measurements, the beam spot used was smaller than the device area to ensure accuracy of the measurement.

Supporting Information

Supporting Information is available from the Wiley Online Library or from the author.

Acknowledgements

The authors gratefully acknowledge the Office of Naval Research (N00014-10-1-0454) for the solution processing of thick film polymer solar cells and the AFOSR (FA9550-09-1-0320) for the PDTG-TPD synthesis.

Received: December 27, 2012
Published online:

[1] L. M. Chen, Z. R. Hong, G. Li, Y. Yang, *Adv. Mat.* **2008**, *21*, 1434.
[2] F. C. Krebs, *Org. Electron.* **2009**, *10*, 761.
[3] C. N. Hoth, S. A. Choulis, P. Schilinsky, C. J. Brabec, *Adv. Mater.* **2007**, *19*, 3973.
[4] F. C. Krebs, S. A. Gevorgyan, J. Alstrup, *J. Mater. Chem.* **2009**, *19*, 5442.
[5] C. E. Small, S. Chen, J. Subbiah, C. Amb, S.-W. Tsang, T.-H. Lai, J. R. Reynolds, F. So, *Nat. Photon.* **2012**, *6*, 115.
[6] S. Chen, C. E. Small, C. M. Amb, J. Subbiah, T.-H. Lai, S.-W. Tsang, J. R. Manders, J. R. Reynolds, F. So, *Adv. Energy Mater.* **2012**, *2*, 1333.
[7] R. R. Søndergaard, M. Hösel, F. C. Krebs, *J. Pol. Sci. Part B: Polym. Phys.* **2013**, *51*, 16.
[8] N. Espinosa, M. Hösel, D. Angmo, F. C. Krebs, *Energy Environ. Sci.* **2012**, *5*, 5117.
[9] A. Hübler, B. Trnovec, T. Zillger, M. Ali, N. Wetzold, M. Mingebach, A. Wagenpfahl, C. Deibel, V. Dyakonov, *Adv. Energy Mater.* **2011**, *1*, 1018.
[10] Y. Galagan, J. M. Rubingh, R. Andriessen, C. C. Fan, P. W. M. Blom, S. C. Veenstra, J. M. Kroon, *Sol. Energy Mater. Sol. Cells* **2011**, *95*, 1339.
[11] T. T. Larsen-Olsen, R. R. Søndergaard, K. Norrman, M. Jørgensen, F. C. Krebs, *Energy Environ. Sci.* **2012**, *5*, 9467.
[12] F. C. Krebs, *Sol. Energy Mater. Sol. Cells* **2009**, *93*, 1636.
[13] F. C. Krebs, *Sol. Energy Mater. Sol. Cells* **2009**, *93*, 465.
[14] M. C. Scharber, D. Mühlbacher, M. Koppe, P. Denk, C. Waldauf, A. J. Heeger, C. J. Brabec, *Adv. Mater.* **2006**, *18*, 789.
[15] J. Y. Kim, K. Lee, N. E. Coates, D. Moses, T.-Q. Nguyen, M. Dante, A. J. Heeger, *Science* **2007**, *317*, 222.
[16] Z. Li, S.-W. Tsang, X. Du, L. Scoles, G. Robertson, Y. Zhang, F. Toll, Y. Tao, J. Lu, J. Ding, *Adv. Funct. Mater.* **2011**, *21*, 3331.
[17] S. Chen, K. R. Choudhury, J. Subbiah, C. M. Amb, J. R. Reynolds, F. So, *Adv. Energy Mater.* **2011**, *1*, 963.
[18] C. M. Amb, S. Chen, K. R. Graham, J. Subbiah, C. E. Small, F. So, J. R. Reynolds, *J. Am. Chem. Soc.* **2011**, *133*, 10062.
[19] A. J. Moulé, J. B. Bonekamp, K. Meerholz, *J. Appl. Phys.* **2006**, *100*, 094503.
[20] V. D. Mihailetchi, H. Xie, B. de Boer, L. M. Popescu, J. C. Hummelen, P. W. M. Blom, L. J. A. Koster, *Appl. Phys. Lett.* **2006**, *89*, 012107.
[21] V. Shrotriya, Y. Yao, G. Li, Y. Yang, *Appl. Phys. Lett.* **2006**, *89*, 063505.
[22] M. Lenes, L. J. A. Koster, V. D. Mihailetchi, P. W. M. Blom, *Appl. Phys. Lett.* **2006**, *88*, 243502.
[23] G. Li, Y. Yao, H. Yang, V. Shrotriya, G. Yang, Y. Yang, *Adv. Funct. Mater.* **2007**, *17*, 1636.
[24] B. C. Thompson, Jean M. J. Fréchet, *Angew. Chem. Int. Ed.* **2008**, *47*, 58.
[25] P. W. M. Blom, V. D. Mihailetchi, L. J. A. Koster, D. E. Markov, *Adv. Mater.* **2007**, *19*, 1551.

[26] J. S. Moon, J. Jo, A. J. Heeger, *Adv. Energy Mater.* **2012**, *2*, 304.
[27] T.-Y. Chu, J. Lu, S. Beaupré, Y. Zhang, J.-R. Pouliot, S. Wakim, J. Zhou, M. Leclerc, Z. Li, J. Ding, Y. Tao, *J. Am. Chem. Soc.* **2011**, *133*, 4250.
[28] J. Peet, J. Y. Kim, N. E. Coates, W. L. Ma, D. Moses, A. J. Heeger, G. G. Bazan, *Nat. Mater.* **2007**, *6*, 497.
[29] J. K. Lee, W. L. Ma, C. J. Brabec, J. Yuen, J. S. Moon, J. Y. Kim, K. Lee, G. C. Bazan, A. J. Heeger, *J. Am. Chem. Soc.* **2008**, *130*, 3619.
[30] S. H. Park, A. Roy, S. Beaupré, S. Cho, N. Coates, J. S. Moon, D. Moses, M. Leclerc, K. Lee, A. J. Heeger, *Nat. Photon.* **2009**, *26*, 297.
[31] V. D. Mihailetchi, J. Wildeman, P. W. M. Blom, *Phys. Rev. Lett.* **2005**, *94*, 126602.
[32] J. Alstrup, M. Jørgensen, A. Medford, F. C. Krebs, *ACS Appl. Mater. Interfaces* **2010**, *2*, 2819.
[33] D. Mühlbacher, M. Scharber, M. Scharber, M. Morana, Z. Zhu, D. Waller, R. Gaudiana, C. Brabec, *Adv. Mater.* **2006**, *18*, 2884.
[34] H. Hoppe, N. Arnold, N. S. Sariciftci, D. Meissner, *Sol. Energy Mat. Sol. Cells* **2003**, **80**, 105.
[35] A. M. Goodman, A. Rose, *J. Appl. Phys.* **1971**, *42*, 2823.
[36] L. Liu, G. Li, *Sol. Energy Mater. Sol. Cells* **2011**, *95*, 2557.
[37] R. A. Street, M. Schoendorf, A. Roy, J. H. Lee, *Phys. Rev. B: Condens. Matter* **2010**, *81*, 205307.
[38] K. R. Choudhury, J. Subbiah, S. Chen, P. M. Beaujuge, C. M. Amb, J. R. Reynolds, F. So, *Sol. Energy Mater. Sol. Cells* **2011**, *95*, 2502.
[39] M. Lenes, M. Morana, C. J. Brabec, P. W. M. Blom, *Adv. Funct. Mater.* **2009**, *19*, 1106.
[40] R. Sokel, R. C. Hughes, *J. Appl. Phys.* **1982**, *53*, 7414.

Adv. Energy Mater. **2013**,
DOI: 10.1002/aenm.201201114